Static and Dynamic Nonlinear In-plane Effect in the Response of a Cantilevered Plate with Tip Mass Load: Theory and Experiment

Luisa Piccolo Serafim^{a,*}, Everett H. Werner^a, Joey Zhou^a, Earl H. Dowell^a

^a Thomas Lord Department of Mechanical Engineering and Materials Science, Duke University, Durham, USA

Abstract

In this paper two nonlinear effects are investigated. One is the effect of the static stiffness nonlinearity in changing the linear dynamic natural frequency and the other is the combination of nonlinear stiffness and nonlinear inertia effects in changing the nonlinear dynamic transient response due to a change in the initial release state of the system. A theoretical model has been developed for a cantilevered thin plate with a range of length to width ratio using beam theory and considering both stiffness and inertial nonlinearities in the model. Lagrange's equation was used to deduce nonlinear inertia and stiffness matrices for a modal representation. Some insights into how these nonlinear components influence the beam response are presented. Measurements with both a hammer test and also a release test of cantilevered thin plates were done using different configurations and tip mass values. Results from static and dynamic analysis using the linear and the nonlinear theoretical model show good agreement between theory and experiment for natural frequencies and the amplitude displacements versus time.

1. Introduction

The discussion of the dynamic response of beams and plates with a tip excitation is well represented in the literature, and several research papers concerning nonlinearities have been presented [1–7]. The present study was inspired by the work of Pai [8], in which the author presents a geometrically exact displacement-based shell theory without singularity problems, considering geometric nonlinearities in the model. Dowell and McHugh [9] use a formulation developed by Novozhilov [10] in which the Eulerian coordinate system is used to describe the beam deflection. Besides presenting their case for two different boundary conditions - clamped-free and free-free cases -, the authors also compare their analytical results using a Lagrange multiplier to consider the inextensibility condition on the beam with experimental data available in the literature, such as the study performed by Tang et al. [6]. Similar to the current work, the dynamic behavior of the beam is assessed for different values of tip mass loads. McHugh and Dowell [11] also use the energy approach for an inextensible cantilevered beam with a follower force acting upon it. These authors evaluate the nonlinear post-critical limit cycle oscillations (LCO) to demonstrate the robustness of the previous nonlinear model based on the work of Novozhilov and validate their model with experimental results from previous studies [5, 12]. Different analytical methods have also been implemented to study nonlinear components in the equation of motion, such as perturbation methods presented by Crespo da Silva and Glynn [1] and Lacarbonara and Yabuno [13], and the harmonic balance method, by Hamdan and Dado [7].

Sayag and Dowell [5] present computational and experimental results from a cantilevered beam under harmonic base excitation, in which the clamped boundary oscillates at a given frequency. The response was measured at the tip of the beam. Moreover, Dowell and McHugh [4] applied Hamilton's principle to derive the equations of motion and also the associated boundary conditions, reaching similar results as from previous studies [2, 6, 14]. Two distinct approaches were presented using the Lagrange multipliers to show insights into the nature of the natural boundary conditions. Tang et al. [15] also present a new inextensible theory of beam and plate deformation. The authors of [9] provide results using computational codes for the static and dynamic nonlinear beam and plate modal equations, showing that the inertia nonlinear force has a significant effect on the dynamic response in the resonant frequency range. Their results show good agreement between inextensible theory and experimental results using cantilevered configurations, exploring both plate and beam formulations. Finally, Muravyov and Rizzi [16] present a computational perspective on the topic with a novel method for determining the nonlinear modal stiffness coefficients using an arbitrary finite element model. These authors present an approach to evaluate the nonlinear stiffness, not requiring the description of the finite element shape functions.

Email address: luisa.piccolo.serafim@duke.edu (Luisa Piccolo Serafim)

^{*}Corresponding author

The current work presents an analytical development for a cantilevered thin panel with a range of length to width ratio using beam theory and introducing the nonlinearities related to in-plane tension and displacement. The analytical results were compared with experimental data collected on a cantilevered thin aluminum plate, measuring the natural frequencies and displacements along its length as they vary with a tip mass that provides both inertial and gravity forces. This study also presents an approximate and exact solution for computing the in-plane displacement as a nonlinear inertia matrix and evaluates the use of such nonlinear matrices in the overall solution. Good agreement between experimental and computational results is shown.

2. Theoretical Model

Figure 1 illustrates the cantilevered beam with a tip force representing the gravity effect of a tip mass positioned at the free end of the structure. The derivation of the equation of motion and the structural matrices were made for the beam considering only bending modes, and the measurements were performed on a range of length to width ratio plate.

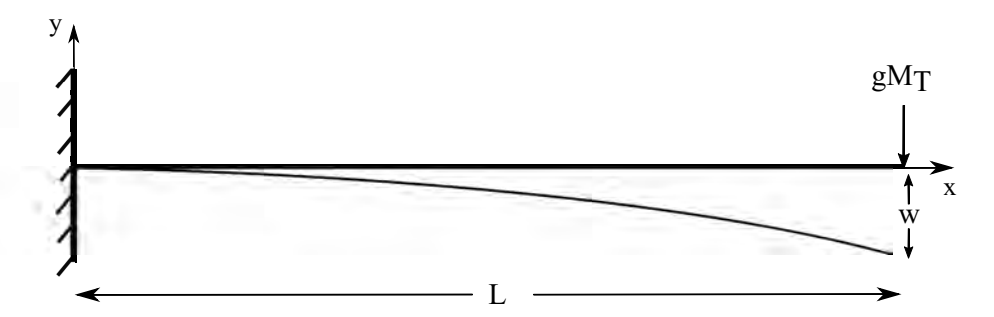


Figure 1: Configuration for a cantilevered beam

2.1. Analytical Modal Formulation

The analytical development was made using the Lagrangian equations:

$$\frac{\partial}{\partial t} \left(\frac{\partial \mathcal{L}}{\partial \dot{q}_i} \right) - \frac{\partial \mathcal{L}}{\partial q_i} = 0, \tag{1}$$

where the Lagrangian is defined as $\mathcal{L} = T - U$ and q_n expresses the generalized coordinates. Only the transverse displacement, w(x,t) is of interest in this study, allowing the use of the kinetic and potential energy only in terms of w, defined by Eq. 2,in which $\psi_n(x)$ is the eigenfunction for a clamped-free beam. Eq. 3 presents the expression for $\psi_n(x)$, which is the linear eigenmode for a cantilevered beam [17]. The physical coordinate w was decomposed in terms of the eigenfunction and the generalized coordinates:

$$w(t,x) = \sum_{n} q_n(t)\psi_n(x). \tag{2}$$

$$\psi(x) = \cos\sqrt{\frac{\omega_n}{a}}x - \cosh\sqrt{\frac{\omega_n}{a}}x + \left(\frac{\sin\sqrt{\frac{\omega_n}{a}}L - \sinh\sqrt{\frac{\omega_n}{a}}L}{\cos\sqrt{\frac{\omega_n}{a}}L - \cosh\sqrt{\frac{\omega_n}{a}}L}\right) \left(\sin\sqrt{\frac{\omega_n}{a}}x - \sinh\sqrt{\frac{\omega_n}{a}}x\right),\tag{3}$$

where $a \equiv \sqrt{EI/m}$. With this expression in hand, one can compute the analytical value for the linear natural frequencies of a cantilevered beam presented in Eq. 4:

$$\omega_1 = (0.597)^2 \frac{\pi^2}{L^2} \sqrt{\frac{EI}{m}},$$

$$\omega_2 = (1.49)^2 \frac{\pi^2}{L^2} \sqrt{\frac{EI}{m}},$$

$$\omega_n = \left(n - \frac{1}{2}\right)^2 \frac{\pi^2}{L^2} \sqrt{\frac{EI}{m}} \quad (n \text{ sufficiently large}).$$
(4)

In the present study, in-plane displacement and tension will be referred to as inertial and stiffness nonlinearities, respectively. They introduce a coupling relationship between different modes when added to the Lagrange's equation,

as presented in the following pages. Their effects on the resonant natural frequencies and the dynamic response are the primary focus. The current study presents the development of nonlinear inertia and stiffness matrices due to such nonlinearities for a cantilevered plate with a tip mass. These nonlinear matrices will be denoted here as $\mathbf{M^{NL}}$ and $\mathbf{K^{NL}}$, respectively. The well-known linear versions of the same matrices, i.e. without the in-plane effects, will be defined here as $\mathbf{M^{L}}$ and $\mathbf{K^{L}}$. Moreover, one can also consider structural damping based on the linear and nonlinear inertia matrices, i.e. $\mathbf{C^{L}}$ and $\mathbf{C^{NL}}$, respectively. The model for the damping matrix is presented in Eq. 5, where ζ_n is the modal structural damping ratio, ω_n is the *n*th natural frequency, calculated by the eigenvalue problem considering only stiffness and inertia components, and M_{nk} is the final mass matrix, which can be linear or nonlinear. Lastly, the static forcing due to the tip mass (M_T) is considered as a generalized force excitation as $Q_n = gM_T |\psi_n|_{x=L}$.

$$C_{nk} = 2\zeta_n \omega_n M_{nk} \tag{5}$$

The following several subsections will present the development for the inertia and stiffness components, focusing on the nonlinear matrices.

2.2. Derivation of the Nonlinear Components

The development of the nonlinear matrices for inertia and stiffness is based on the assumption that the generalized coordinate due to the tip mass loading gM_T can be expressed in terms of a static (q_{n_s}) and a dynamic component $(\hat{q}_n(t))$:

$$q_n(t) = \hat{q}_n(t) + q_{n_n}. \tag{6}$$

Considering this decomposition of $q_n(t)$, the derivation of the nonlinear matrices due to the in-plane nonlinearities inserted in the Lagrangian analysis is presented as follows:

2.2.1. Nonlinear Stiffness Matrix

The nonlinear stiffness component is calculated from the expression for potential energy, as presented in [6, 9]:

$$U = \frac{1}{2} \int_{0}^{L} EIw_{xx}^{2} \left(1 + w_{x}^{2}\right) dx. \tag{7}$$

Substituting Eq. 2 and 6 into 7, the nonlinear stiffness component becomes a 4-D matrix due to the extra derivatives on the eigenfunctions associated with the added nonlinear tension, as presented in Eq. 8:

$$U = \frac{1}{2} \sum_{n} \sum_{m} q_n q_m \left(\int_0^L EI\psi_{n_{xx}} \psi_{m_{xx}} dx \right) + \frac{1}{2} \sum_{n} \sum_{m} \sum_{r} \sum_{t} q_n q_m q_r q_t \left(\int_0^L EI\psi_{n_{xx}} \psi_{m_{xx}} \psi_{r_x} \psi_{t_x} dx \right). \tag{8}$$

The final expression for the overall potential energy in Eq. 8 can be represented by a summation of the linear (U^L) and nonlinear (U^{NL}) components. Based on the assumption made in Eq. 6, and considering only terms related to the dynamic portion of the generalized coordinate, \hat{q}_n , the linear potential energy component in the Lagrange equation is presented in Eq. 9:

$$\frac{\partial U^L}{\partial \hat{q}_i} = \sum_n \hat{q}_n \int_0^L EI\psi_{i_{xx}} \psi_{n_{xx}} dx, \tag{9}$$

while the nonlinear portion of the potential energy has both the dynamic and static terms from the generalized coordinates. Considering \hat{q}_n small enough and retaining only linear terms related to \hat{q}_n , the final nonlinear potential energy component can be added to the Lagrange equation from Eq. 10:

$$\frac{\partial U^{NL}}{\partial \hat{q}_i} = \sum_{r} \sum_{t} 3q_{r_s} q_{t_s} \hat{q}_n \int_0^L EI\left(\psi_{i_{xx}} \psi_{n_{xx}} \psi_{r_x} \psi_{t_x} + \psi_{n_{xx}} \psi_{r_{xx}} \psi_{i_x} \psi_{t_x}\right) dx. \tag{10}$$

2.2.2. Nonlinear Inertia Matrix

90

The expression for kinetic energy can also be written with nonlinear components from the in-plane displacement u, presented in Eq. 11:

$$T = \frac{1}{2} \int_0^L m \left(\dot{\hat{w}}^2 + \dot{\hat{u}}^2 \right) dx + \left. \frac{M_T}{2} \left(\hat{w}^2 + \dot{\hat{u}}^2 \right) \right|_{x=L}. \tag{11}$$

Assuming an inextensible beam, which relates u to w as presented in Eq. 12, the development of the nonlinear inertial matrix from the kinetic energy can be made with an approximation for the time-derivative of the dynamic portion of the in-plane displacement \hat{u} , or with its exact expression.

$$\frac{\partial u}{\partial x} + \frac{1}{2} \left(\frac{\partial w}{\partial x} \right)^2 = 0. \tag{12}$$

Both options for the nonlinear inertia component will be presented here:

Approximation Solution for the Nonlinear Inertia Matrix

The approximation for \hat{u} is first considered through the assumption that $\frac{\partial w_s}{\partial x}$ is constant with respect to x:

$$\dot{\hat{u}} = \left(\frac{\partial w_s}{\partial x}\right)\dot{\hat{w}} = \left(\sum_r q_r \psi_{r_x}\right) \left(\sum_n \dot{\hat{q}}_n \psi_n\right). \tag{13}$$

Substitute Eqs. 2 and 13 in Eq. 11, and regrouping the terms:

$$T = \frac{1}{2} \sum_{n} \sum_{m} \dot{\hat{q}}_{n} \dot{\hat{q}}_{m} \left(\int_{0}^{L} m \psi_{n} \psi_{m} dx + M_{T} \psi_{n} \psi_{m} |_{x=L} \right) + \frac{1}{2} \sum_{n} \sum_{m} \sum_{r} \sum_{t} \dot{\hat{q}}_{n} \dot{\hat{q}}_{m} q_{r_{s}} q_{t_{s}} \left(\int_{0}^{L} m \psi_{n} \psi_{m} \psi_{r_{x}} \psi_{t_{x}} dx + M_{T} \psi_{n} \psi_{m} \psi_{r_{x}} \psi_{t_{x}} |_{x=L} \right).$$

$$(14)$$

Similar to the potential energy, the nonlinear portion of the kinetic energy is organized as a 4-D structure due to the added in-plane displacement. Recall that q_{r_s} and q_{t_s} are static displacement due to the gravity force. Similarly to Subsection 2.2.1, the kinetic energy is separated into linear and nonlinear terms, being written as the summation of a linear (T^L) and a nonlinear (T^{NL}) portion. Applying the partial derivative in terms of \dot{q}_i , and the time derivative in both the linear and nonlinear portions of the kinetic energy, Eqs. 15 and 16 define the modal components to be used in the Lagrange equation.

$$\frac{d}{dt} \left(\frac{\partial T^L}{\partial \dot{q}_i} \right) = \sum_n \ddot{q}_n \left(\int_0^L m \psi_i \psi_n dx + M_T \psi_i \psi_n \big|_{x=L} \right), \tag{15}$$

$$\frac{d}{dt} \left(\frac{\partial T^{NL}}{\partial \dot{q}_i} \right) = \sum_n \sum_r \sum_t \ddot{q}_n q_{r_s} q_{t_s} \left(\int_0^L m \psi_i \psi_n \psi_{r_x} \psi_{t_x} dx + M_T \psi_i \psi_n \psi_{r_x} \psi_{t_x} \big|_{x=L} \right).$$
(16)

Exact Solution for the Nonlinear Inertia Matrix

Rewriting Eq. 11, but now considering the exact definition of $\dot{\hat{u}}$, with $\frac{\partial w_s}{\partial x}$ as part of the integrand function, as presented in Eq. 17:

$$\dot{\hat{u}} = -\int_0^x \left(\frac{\partial w_s}{\partial x^*}\right) \left(\frac{\partial \dot{w}}{\partial x^*}\right) dx^* = -\int_0^x \left(\sum_r q_r \psi_{r_{x^*}}\right) \left(\sum_n \dot{\hat{q}}_n \psi_{n_{x^*}}\right) dx^*. \tag{17}$$

Substitute Eqs. 2 and 17 in Eq. 11 considering only the dynamic portion of q_n , since there is no time derivative for the static portion of the displacement. Expanding and regrouping the terms in the kinetic energy expression, one can separate the linear and the nonlinear components:

$$T = \frac{1}{2} \sum_{n} \sum_{m} \dot{\hat{q}}_{n} \dot{\hat{q}}_{m} \left(\int_{0}^{L} m \psi_{n} \psi_{m} dx + M_{T} \psi_{n} \psi_{m} |_{x=L} \right) + \frac{1}{2} \sum_{n} \sum_{m} \sum_{r} \sum_{t} \dot{\hat{q}}_{n} \dot{\hat{q}}_{m} q_{r_{s}} q_{t_{s}} \left[\int_{0}^{L} m \left(\int_{0}^{x} \psi_{n_{x^{*}}} \psi_{r_{x^{*}}} dx^{*} \right) \left(\int_{0}^{x} \psi_{m_{x^{*}}} \psi_{t_{x^{*}}} dx^{*} \right) dx + \frac{M_{T}}{2} \left(\int_{0}^{x} \psi_{n_{x^{*}}} \psi_{r_{x^{*}}} dx^{*} \right) \left(\int_{0}^{x} \psi_{m_{x^{*}}} \psi_{t_{x^{*}}} dx^{*} \right) \Big|_{x=L} \right].$$

$$(18)$$

Deriving Eq. 18 in terms of \dot{q}_i and in time provides the results needed in the Lagrange equation:

$$\frac{d}{dt} \left(\frac{\partial T^L}{\partial \dot{q}_i} \right) = \sum_n \ddot{q}_n \left(\int_0^L m \psi_i \psi_n dx + M_T \psi_i \psi_n \big|_{x=L} \right), \tag{19}$$

$$\frac{d}{dt} \left(\frac{\partial T^{NL}}{\partial \dot{q}_{i}} \right) = \sum_{n} \sum_{r} \sum_{t} \ddot{q}_{n} q_{r_{s}} q_{t_{s}} \left[\int_{0}^{L} m \left(\int_{0}^{x} \psi_{i_{x^{*}}} \psi_{r_{x^{*}}} dx^{*} \right) \left(\int_{0}^{x} \psi_{n_{x^{*}}} \psi_{t_{x^{*}}} dx^{*} \right) dx + M_{T} \left(\int_{0}^{x} \psi_{i_{x^{*}}} \psi_{r_{x^{*}}} dx^{*} \right) \left(\int_{0}^{x} \psi_{n_{x^{*}}} \psi_{t_{x^{*}}} dx^{*} \right) \Big|_{x=L} \right],$$
(20)

2.3. Final Solution

Solving Eq. 1 with the components derived in the previous subsections allows the definition of the linear and nonlinear matrices for the system. For the nonlinear stiffness matrix:

$$K_{i,n}^{NL} = \sum_{r} \sum_{t} (3q_{r_s}q_{t_s}) \int_0^L EI\left(\psi_{i_{xx}}\psi_{n_{xx}}\psi_{r_x}\psi_{t_x} + \psi_{n_{xx}}\psi_{r_{xx}}\psi_{i_x}\psi_{t_x}\right) dx \tag{21}$$

For the nonlinear inertia matrix, there are two options to follow through. The differences between them will be explored later. The approximate version is given in Eq. 22 and the exact solution in Eq. 23.

$$M_{i,n}^{NL}_{approx} = \sum_{r} \sum_{t} q_{r_s} q_{t_s} \left(\int_0^L m \psi_i \psi_n \psi_{r_x} \psi_{t_x} dx + M_T \psi_i \psi_n \psi_{r_x} \psi_{t_x} \big|_{x=L} \right), \tag{22}$$

$$M_{i,n}^{NL}{}_{exact} = \sum_{r} \sum_{t} q_{r_{s}} q_{t_{s}} \left[\int_{0}^{L} m \left(\int_{0}^{x} \psi_{i_{x^{*}}} \psi_{r_{x^{*}}} dx^{*} \right) \left(\int_{0}^{x} \psi_{n_{x^{*}}} \psi_{t_{x^{*}}} dx^{*} \right) dx + M_{T} \left(\int_{0}^{x} \psi_{i_{x^{*}}} \psi_{r_{x^{*}}} dx^{*} \right) \left(\int_{0}^{x} \psi_{n_{x^{*}}} \psi_{t_{x^{*}}} dx^{*} \right) \Big|_{x=L} \right].$$

$$(23)$$

It is important to recall that in this study, the beam has a tip mass. Therefore, it is necessary to add the effect of this tip mass on the structure to the final inertia and stiffness matrices by making similar steps but considering a fixed position at x = L.

2.3.1. Eigenvalue Method

Although this study considers nonlinear matrices for mass and stiffness, it is possible to construct an eigenvalue problem to calculate the structure's natural frequencies. Using Eq. 24 to represent the dynamic component of the generalized coordinate, the eigenvalue problem without nonlinearities is expressed by Eq. 25 while Eq. 26 presents the implementation considering the in-plane nonlinearities in the equation of motion.

$$\hat{q} = \bar{q}e^{i\omega t} \tag{24}$$

$$\left(-\omega^{2}\left[\mathbf{M}^{L}\right] + \left[\mathbf{K}^{L}\right]\right)\bar{q}e^{i\omega t} = 0, \tag{25}$$

$$\left(-\omega^{2}\left(\left[\mathbf{M}^{\mathbf{L}}\right]+\left[\mathbf{M}^{\mathbf{NL}}\right]\right)+\left(\left[\mathbf{K}^{\mathbf{L}}\right]+\left[\mathbf{K}^{\mathbf{NL}}\right]\right)\right)\bar{q}e^{i\omega t}=0,$$
(26)

2.3.2. Time-marched Simulations

Similarly, the nonlinear dynamic response of the system can be calculated solving the time dependent ODE with the damping matrix defined by Eq. 5, for both the cases with linear, Eq. 27, and nonlinear matrix components, Eq. 28:

$$\left[\mathbf{M}^{\mathbf{L}}\right] \left\{\ddot{q}\right\} + \left[\mathbf{C}^{\mathbf{L}}\right] \left\{\dot{q}\right\} + \left[\mathbf{K}^{\mathbf{L}}\right] \left\{\bar{q}\right\} = \left\{Q\right\},\tag{27}$$

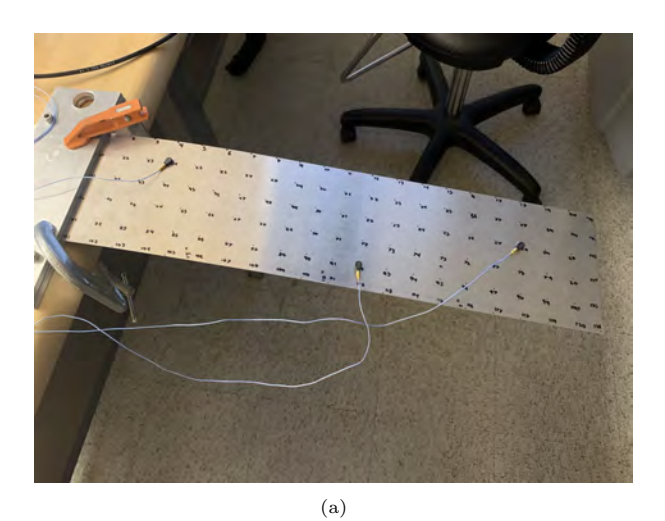
$$([\mathbf{M}^{\mathbf{L}}] + [\mathbf{M}^{\mathbf{NL}}]) \{\ddot{q}\} + [\mathbf{C}^{\mathbf{NL}}] \{\dot{q}\} + ([\mathbf{K}^{\mathbf{L}}] + [\mathbf{K}^{\mathbf{NL}}]) \{\bar{q}\} = \{Q\}$$
(28)

3. Results

The results from the analytical model were compared with experimental results as part of the present study.

3.1. Experimental configuration

To capture the effects of the inertial and stiffness nonlinearities from the real plate, two measurements were performed on a 6061 Aluminum thin plate. The study began with a hammer test, represented in Fig. 2.a, where three accelerometers were placed in carefully selected positions on the surface to capture the natural frequencies of the plate with magnetic tip mass loads on the free end. The second measurement performed was a release test, Fig 2.b, in which a laser system was used for the data acquisition measuring the displacement at a specific location. The plate, with the magnetic tip mass load, was released from its stationary position without the tip mass. In this case, the measurement was performed at the middle of the plate's length in order to keep the displacement within the laser's range. For both measurements, the plate was clamped between two 1/2-inch thick metal plates and held in place using two bar clamps, and the tip mass was equally distributed along the width to avoid torsion modes. Table 1 presents the dimensions and material properties considered. For this study, the different lengths considered are based on the nominal value presented in Table 1 and the aspect ratio is defined as AR = Length/Width.



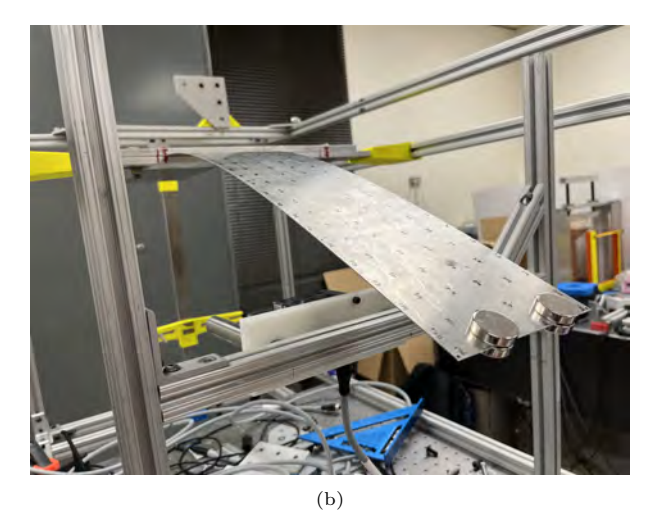


Figure 2: Setup for: a) Hammer test, and b) Release test

Parameters	Value
Thickness [in]	0.032
Length [in]	10
Width [in]	5
E [GPa]	69
$\rho [\mathrm{kg/m^3}]$	2700
ν	0.3

Table 1: Material properties and plate dimensions

3.2. Comparison of solutions: Stiffness and Inertia

The first comparison presented is between results obtained using the approximate and the exact solutions when computing the nonlinear effect of the in-plane displacement. As presented in Subsection 2.2.2, the approximate method is based on the assumption that the static displacement does not vary along the span, being considered constant in the analytical development. Figure 3 shows the comparison between the two methods for a 5:1 plate, which is the longest configuration analyzed in this study. One can see that, even for this configuration with a relatively large aspect ratio, the difference between the approximate method and the exact one is small. As the length of the plate increases, it is expected the difference between the methods will increase, as presented in Fig. 4, especially when evaluating higher modes, which tend to be more sensitive to nonlinear effects. However, as the length grows, the tip mass value that causes the structure to buckle decreases. Moreover, for longer plates, the ratio of tip deflection and the panel thickness becomes so large that the linear dynamic solution approach here presented is no longer applicable.

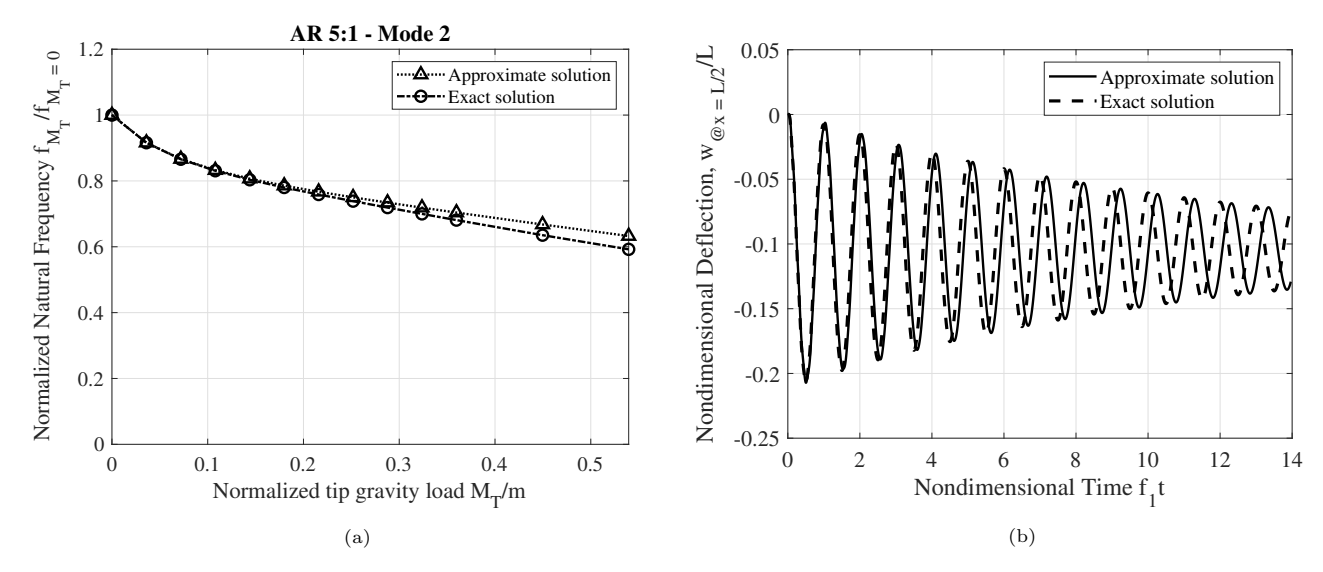


Figure 3: Comparison between the approximate and the exact solution for the nonlinear in-plane displacement. a) Second mode natural frequencies of a 5:1 AR Plate for a range of tip mass, and b) dynamic displacement for a 5:1 AR plate with 78.3 g of tip mass. The time scale was nondimensionalized by the first natural frequency calculated using the in-plane nonlinearities in the solution

Considering now the comparison between the dynamic displacement, Fig. 3.b, the results from the two methods start to diverge later in time. The amplitude of both methods, however, remains very similar. Therefore, it is possible to conclude that the simpler inertial approximation can be used for a short period of time when evaluating the dynamic displacement, or for a small mass tip variation when computing the natural frequencies. The same can not be said for longer time ranges or larger excitation loads. However, for the case presented in this study, it is not computationally demanding to implement Eq. 23 rather than Eq. 22, which led to the use of the exact inertial solution for the following results.

Figure 4 presents natural frequencies for the plate considering different components in the final equation of motion: linear and/or nonlinear inertia and stiffness matrices. Here it becomes clear that the nonlinear stiffness and nonlinear inertia have opposite effects and balance each other in the model considering both nonlinearities, as already noted in [9] as far as the natural frequencies are concerned.

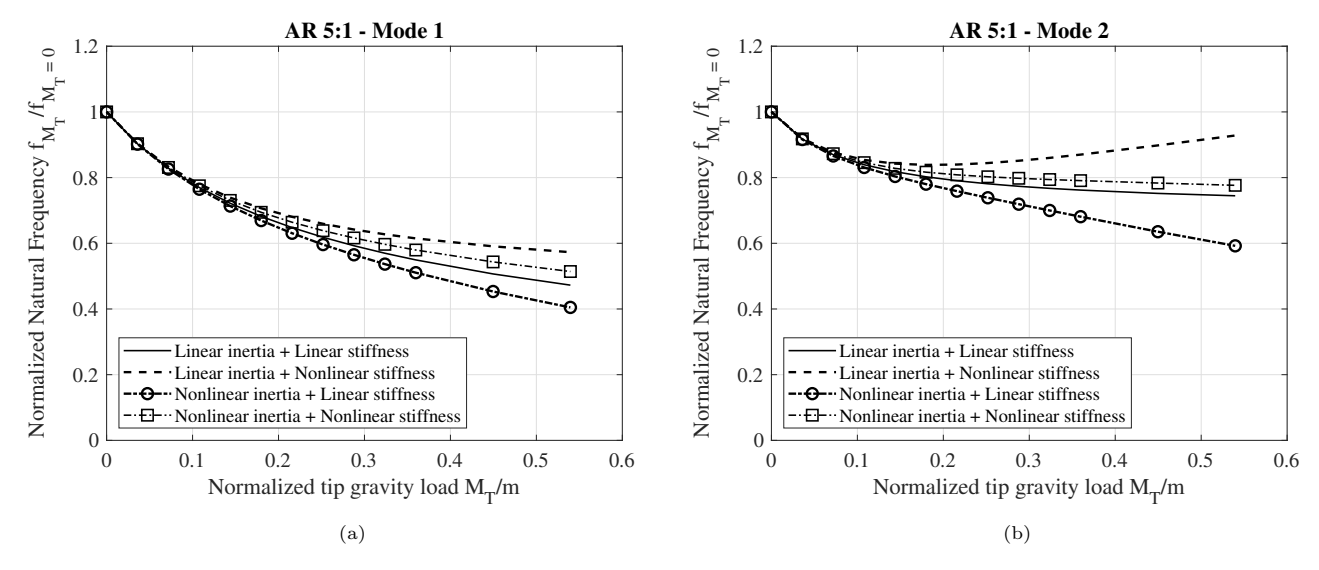


Figure 4: Comparison of natural frequencies when considering or not the in-plane nonlinearities in the final solution. a) First mode natural frequencies of a 5:1 AR Plate for a range of tip mass, and b) Second mode natural frequencies of a 5:1 AR Plate for a range of tip mass

3.3. Natural frequencies

Now comparing the analytical formulation with experimental results, Figs. 5 and 6 show the agreement between the implementation using only linear matrices by contrast with the solution considering the nonlinearities in the problem. One can observe that as the AR increases, the agreement between experimental and theory improves, which can be associated with the approximation of the analytical model developed in this study using the beam model for a plate with an increased aspect ratio. However, since the range of tip mass allowed by the structure before buckling is small, there are no strong conclusions from comparing theory and experiment about the differences between models with or without nonlinearities. Nevertheless, the computational results show that when assessing the nonlinear inertia and stiffness effects individually, they are important. Thus another experiment was designed to assess nonlinear dynamic response.

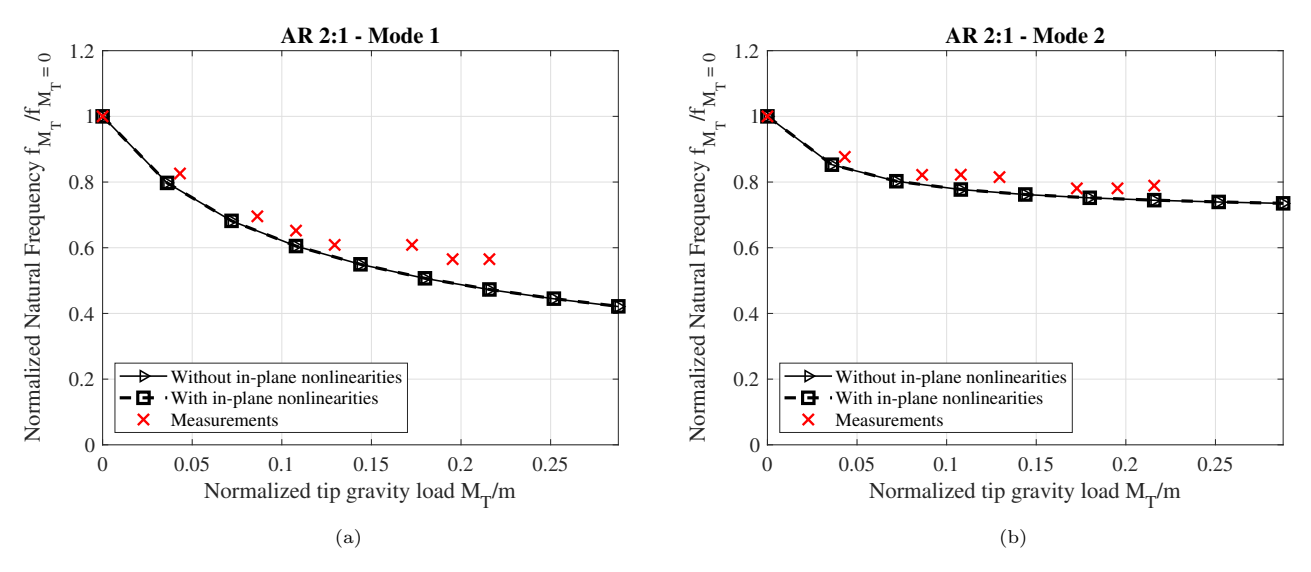


Figure 5: Comparison of natural frequencies when considering or not the in-plane nonlinearities in the final solution. a) First mode natural frequencies of a 2:1 AR Plate for a range of tip mass, and b) Second mode natural frequencies of a 2:1 AR Plate for a range of tip mass

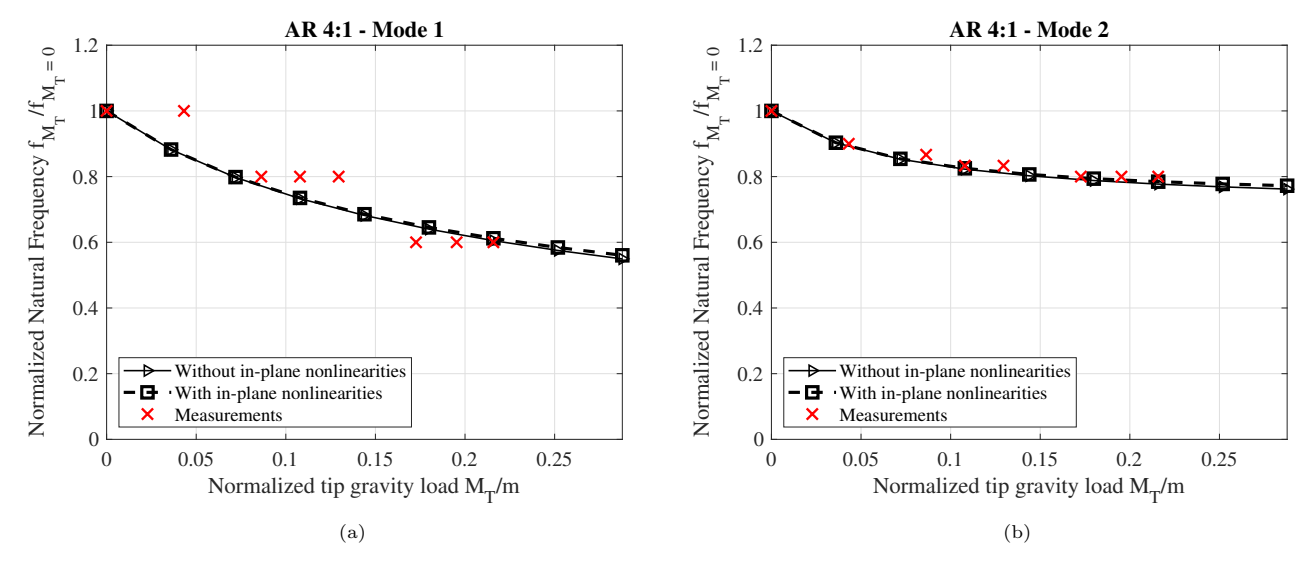


Figure 6: Comparison of natural frequencies when considering or not the in-plane nonlinearities in the final solution. a) First mode natural frequencies of a 4:1 AR Plate for a range of tip mass, and b) Second mode natural frequencies of a 4:1 AR Plate for a range of tip mass

3.4. Nonlinear Static and Dynamic Displacement Results

It is known that the static displacement is only affected by the stiffness in the system. Thus, the only nonlinear effect presented in the static solution is the one that originated from the in-plane tension. To provide more information on both in-plane effects, i.e. stiffness and inertia, one can analyze the displacement of the plate in time, which considers both the structure's nonlinear inertia and stiffness in the calculation and the experiment.

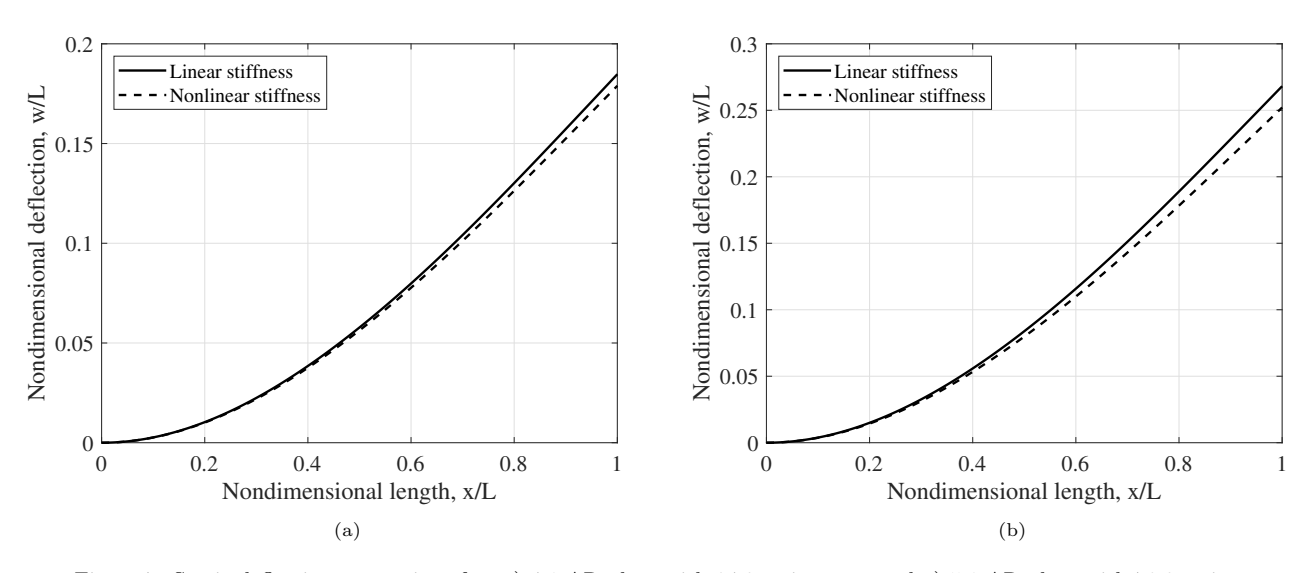


Figure 7: Static deflection comparison for: a) 4:1 AR plate with 84.3 g tip mass, and a) 5:1 AR plate with 78.3 g tip mass

When comparing the difference between the amplitude displacements from the static and dynamic results of the same plate with the same mass tip value, presented in Figs. 7.a and 8, one can see that the added nonlinear in-plane displacement in the solution does not have a large contribution to the dynamic displacement since both the linear and nonlinear formulations present nearly the same amplitude in the figure. However, the dynamic response in Fig. 8 shows a larger difference between the linear and nonlinear formulations than the static result. It is then possible to conclude that the analysis of the transient dynamic displacement time history of the plate under a release excitation can provide a much more thorough assessment of the nonlinear dynamic behavior of the structure than by evaluating the static deflection or the natural frequencies separately. Moreover, the nonlinearity introduced by both inertia and stiffness is responsible for the final displacement amplitude. This conclusion will also be better supported by comparing the theoretical model results with experimental results.

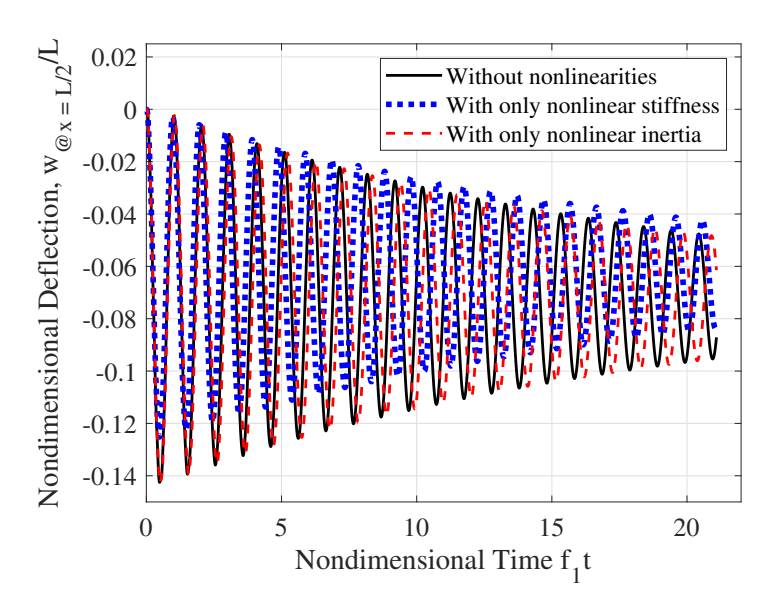


Figure 8: Dynamic displacement at half length of a 4:1 AR plate with 84.3 g tip mass. The time scale was nondimensionalized by the first natural frequency calculated using the in-plane nonlinearities in the solution

3.5. Dynamic Displacement of a Beam/Plate Released from Rest (Horizontal Position)

Figure 9.a presents the results for the 4:1 plate with a tip mass of 84.3 g, and Fig. 9.b presents the same information for a 5:1 plate with a 78.3 g of tip mass. Evaluating only the amplitude of the displacement at the middle of the plate, disregarding the comparison between frequencies already presented in Sub-section 3.3, the results show that the presence of both in-plane nonlinearities, i.e. the nonlinear inertia and nonlinear stiffness matrices, decrease the overall displacement when compared with the linear model. In addition, the agreement between experimental data and analytical results is good and one can conclude that the presented analytical implementation succeeds in replicating the nonlinear dynamic behavior of a cantilevered plate with a range of aspect ratio using a beam implementation for the structural matrices.

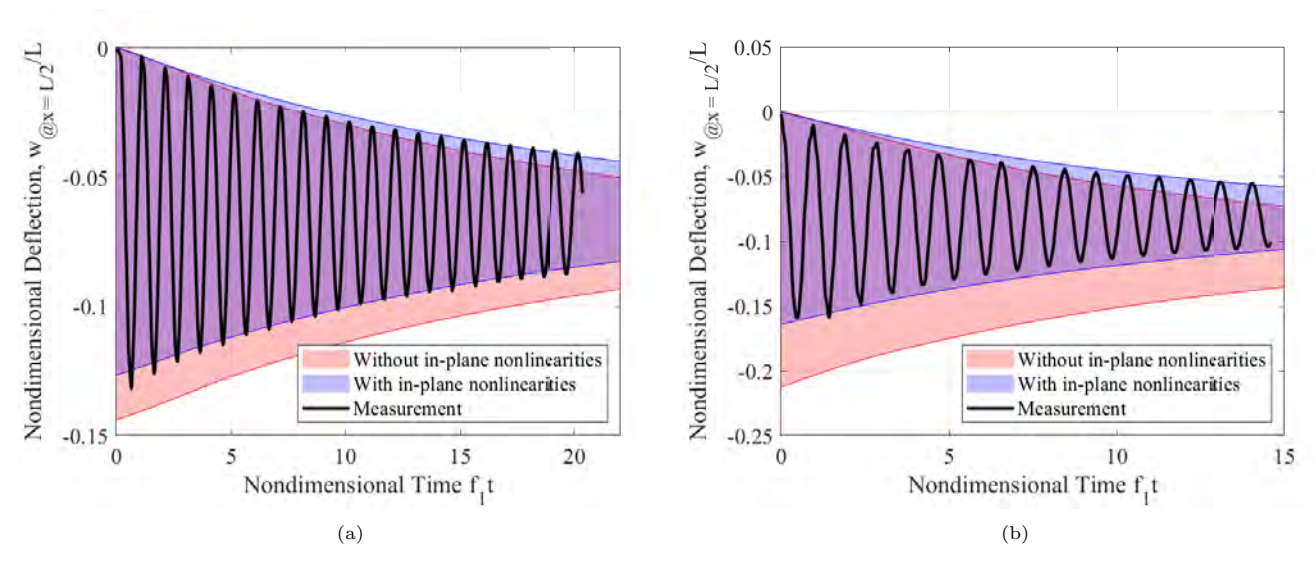


Figure 9: Comparison of the overall dynamic displacement from theory and experiment at half length of a: a) 4:1 AR plate 84.3 g tip mass, and b) 5:1 AR plate with 78.3 g tip mass. The time scale was nondimensionalized by the first natural frequency calculated using the in-plane nonlinearities in the solution

4. Conclusion

A computational study of a cantilevered beam under the excitation of tip mass was performed and compared with experimental results from a cantilevered plate with a range of aspect ratio. In terms of the computation of

the in-plane displacement to form a nonlinear inertia matrix, both an approximate and the exact solution for the formulation were presented, and the comparison between their performance and their use in the model was noted. In addition, the results considering only in-plane tension and/or in-plane displacement, which are computed as nonlinear stiffness and nonlinear inertia matrices respectively, were presented for comparison.

It was found that comparing only the natural frequencies, the effects of in-plane stiffness and inertia tend to cancel each other and there is a little difference between the implementation of the theoretical model with and without these nonlinearities, as earlier investigators had also concluded [9]. However, by considering the time history of a cantilevered plate released from rest, it was found that the presence of both these nonlinearities in the solution decreases the dynamic response. The experiments conducted in this study and the comparison made with the theoretical implementation showed that the method presented here can effectively represent the nonlinear behavior of thin plates with a range of length to width ratio by using beam theory. The torsional effects were not considered in this study.

References

225

230

240

- [1] M. Da Silva, Non-linear flexural-flexural-torsional-extensional dynamics of beams i. formulation, International Journal of Solids and Structures 24 (12) (1988) 1225–1234. doi:https://doi.org/10.1016/0020-768 3(88)90087-X.
- [2] M. R. M. C. da Silva, C. C. Glynn, Nonlinear flexural-flexural-torsional dynamics of inextensional beams. ii. forced motions, Journal of Structural Mechanics 6 (4) (1978) 449–461. doi:10.1080/03601217808907349.
 - [3] S. N. Mahmoodi, N. Jalili, S. Khadem, An experimental investigation of nonlinear vibration and frequency response analysis of cantilever viscoelastic beams, Journal of Sound and Vibration 311 (2008) 1409–1419. doi:10.1016/j.jsv.2007.09.027.
- [4] E. Dowell, K. McHugh, Equations of motion for an inextensible beam undergoing large deflections, Journal of Applied Mechanics 83 (5). doi:10.1115/1.4032795.
 - [5] M. R. Sayag, E. H. Dowell, Linear versus nonlinear response of a cantilevered beam under harmonic base excitation: Theory and experiment, Journal of Applied Mechanics 83 (10). doi:10.1115/1.4034117.
 - [6] D. Tang, M. Zhao, E. H. Dowell, Inextensible beam and plate theory: Computational analysis and comparison with experiment, Journal of Applied Mechanics 81 (6). doi:10.1115/1.4026800.
 - [7] M. N. Hamdan, M. H. F. Dado, Large Amplitude Free Vibrations of a Uniform Cantilever Beam Carrying AN Intermediate Lumped Mass and Rotary Inertia, Journal of Sound Vibration 206 (2) (1997) 151–168. doi:10.1006/jsvi.1997.1081.
 - [8] P. Pai, R. Chapman, Z. Feng, Geometrically exact displacement-based shell theory, Thin-Walled Structures 70 (2013) 1–18. doi:10.1016/j.tws.2013.04.010.
 - [9] K. McHugh, E. Dowell, Nonlinear responses of inextensible cantilever and free-free beams undergoing large deflections, Journal of Applied Mechanics 85 (5). doi:10.1115/1.4039478.
 - [10] V. V. Novozhilov, Foundations of the nonlinear theory of elasticity, Graylock Press, Rochester, N.Y., 1953.
- [11] K. A. McHugh, E. H. Dowell, Nonlinear Response of an Inextensible, Cantilevered Beam Subjected to a Nonconservative Follower Force, Journal of Computational and Nonlinear Dynamics 14 (3), 031004. doi: 10.1115/1.4042324.
 - [12] D. Tang, S. C. Gibbs, E. H. Dowell, Nonlinear aeroelastic analysis with inextensible plate theory including correlation with experiment, AIAA Journal 53 (5) (2015) 1299–1308. doi:10.2514/1.J053385.
- [13] W. Lacarbonara, H. Yabuno, Refined models of elastic beams undergoing large in-plane motions: Theory and experiment, International Journal of Solids and Structures 43 (17) (2006) 5066–5084. doi:https://doi.org/10.1016/j.ijsolstr.2005.07.018.
 - [14] L. G. Villanueva, R. B. Karabalin, M. H. Matheny, D. Chi, J. E. Sader, M. L. Roukes, Nonlinearity in nanomechanical cantilevers, Physical Review B 87 (2). doi:10.1103/physrevb.87.024304.

- [15] D. Tang, S. C. Gibbs, E. H. Dowell, Nonlinear aeroelastic analysis with inextensible plate theory including correlation with experiment, AIAA Journal 53 (5) (2015) 1299–1308. doi:10.2514/1.J053385.
 - [16] A. A. Muravyov, S. A. Rizzi, Determination of nonlinear stiffness with application to random vibration of geometrically nonlinear structures, Computers Structures 81 (15) (2003) 1513–1523. doi:10.1016/s0045-79 49(03)00145-7.
 - [17] A. W. Leissa, Vibration of Plates, NASA Report No. SP-160, 1969.